Submitted to

XXII International Symposium on Lepton-Photon Interactions at High Energy, June 30, 2005, Uppsala

Abstract: **409**

Parallel Session **Flavor physics** and **QCD and hadron structure**

www-h1.desy.de/h1/www/publications/conf/conf_list.html

Study of Jet Shapes in Charm Photoproduction at HERA

H1 Collaboration

Abstract

Charm dijet events are investigated in the photoproduction kinematic range in ep collisions at HERA. One jet is tagged by a muon as being initiated by a charm quark. The shape of the other jet is studied in order to distinguish if it is initiated by a quark or a gluon in order to shed light on the production mechanism of charm events in ep collisions. The data were collected with the H1 Experiment in the years 1999-2000. The jet shapes are studied as function of kinematic variables such as the transverse momentum, energy and pseudorapidity of the jet and the quantity x_γ^{obs}. The shapes are found to be well described by the leading order plus parton shower Monte Carlo simulation PYTHIA in the region of large $x_\gamma^{obs} > 0.75$, where according to the simulation the jets are dominantly charm quark initiated. Deviations are observed for small $x_\gamma^{obs} < 0.75$, where resolved photon events are expected to contribute significantly and more gluon jets are expected. No such deviations are observed in a dijet photoproduction sample without muon requirements, which is dominated by light quark production.

1 Introduction

Charm production in ep collisions at HERA is dominated by photon gluon fusion processes (fig. 1). In photoproduction the exchanged photon is quasi-real and in addition to direct photon processes (fig. 1a), resolved photon processes (fig. 1b-d) can contribute significantly, where the photon acts as a source of quarks and gluons which participate in the hard interaction. A key question is to which extent the charm production can be attributed to the so called c-excitation processes (fig. 1c-d), where the c quark is a constituent of the resolved photon. In perturbative QCD at leading order only the c-excitation processes produce a hard gluon in addition to a hard charm quark, while the direct photon (fig. 1a) and other hadron-like resolved processes (fig. 1b) lead to the production of a $c\bar{c}$ pair.

The aim of the present study is the distinction of the charm quark-pair component from the charm quark-gluon events. In this analysis dijet events in which one jet is tagged as being initiated by the charm quark are used to study the shapes of the other jet. Quark and gluon initiated jets are expected to have different 'shapes', i.e. a different distribution of the energy flow as a function of the radial distance from the jet axis. Such differences have been observed previously between jets initiated by light quarks and by gluons [1], while b quark initiated jets were found to have almost the same shape as gluon jets.

2 Experimental Method

The jet shapes are studied using the variable:

$$\psi(r) = \frac{p_t^{jet}(r)}{p_t^{jet}(r = R)}. \tag{1}$$

$\psi(r)$, 'the integrated jet shape', is the fraction of the jet transverse momentum deposited within a cone of the radius r around the jet axis relative to the total transverse momentum of the jet within R (figure 2). Transverse momenta are measured with respect to the beam axis. The radius is defined as $r = \sqrt{\Delta\eta^2 + \Delta\phi^2}$, where $\Delta\eta$ and $\Delta\phi$ are the distances of the individual particles forming the jet to the jet axis in pseudorapidity[1] η and azimuthal angle ϕ, respectively. The variable $\psi(r)$ is averaged over the jets of the selected event sample

$$\langle\psi(r)\rangle = \frac{1}{N_{jets}} \sum_{jets} \psi(r).$$

The integrated jet shape is studied as a function of r at a given value of R (we choose $R = 1$ for the analysis, since the same value is chosen in the jet algorithm). Due to differences in the formation processes (fig. 3) of charm and gluon jets the latter are expected to be broader and contain more particles [2]. Hence the distribution of $\psi(r)$ is expected to be different. For gluons the full transverse momentum is reached more slowly and at a given radius the value

[1]The pseudorapidity η of an object with polar angle θ is given by $\eta = -\ln\ \tan(\theta/2)$, where θ is measured with respect to the z-axis given by the proton beam direction.

is on average smaller. Fig. 4 shows the differences in the $\psi(r)$ distributions of light quark and gluon jets as observed for high jet energies in e^+e^- collisions at LEP [1]. The jet energies in the present analysis are lower but still high enough to expect significant differences in the jet shapes of gluon and charm initiated jets, according to the Monte Carlo Simulation (e.g. using the PYTHIA [3] generator).

3 Detector Description

The H1 detector is described in detail in [4]. Charged particles emerging from the interaction region are measured by the central tracking detector (CTD) in the pseudorapidity range $-1.74 < \eta < 1.74$. The CTD comprises two large cylindrical drift chambers (central jet chambers) and two z-chambers arranged concentrically around the beam-line within a solenoidal magnetic field of 1.15 T. The CTD also provides triggering information based on track segments in the r-ϕ plane from the CJC and the z-position of the vertex from a double layer of multi-wire proportional chambers.

The CJC tracks are linked with hits in the Central Silicon Tracking Detector (CST) [6], which consists of two cylindrical layers of silicon strip detectors, surrounding the beam pipe at radii of $R = 57.5$ mm and $R = 97$ mm from the beam axis. These double-sided silicon detectors with readout strip pitches of 50 μm and 88 μm provide resolutions of 12 μm in r-ϕ and 25 μm in z. Average hit efficiencies reach values of 97 (92)% in r-ϕ (z). For tracks with CST hits in both layers the transverse distance of closest approach (dca) of the track to the interaction point can be measured with a resolution of $\sigma_{dca} \approx 33\ \mu\text{m} \oplus 90\ \mu\text{m}/p_T[\text{GeV}]$. The first term represents the intrinsic resolution and includes the uncertainty of the CST alignment. The second term gives the contribution from multiple scattering in the beam pipe.

The energies of final state particles are measured using CTD+CST track information and measurements of the energy deposited in the liquid argon (LAr) calorimeter, which surrounds the tracking chambers and covers the range $-1.5 < \eta < 3.4$. The backward region ($-4.0 < \eta < -1.4$) is covered by a lead–scintillating fibre calorimeter (SPACAL) with electromagnetic and hadronic sections. The calorimeters are surrounded by the iron return yoke of the solenoidal magnet. The tracks of muons which penetrate the main detector are reconstructed using limited streamer tubes placed within the iron in the range $-2.5 < \eta < 3.4$. The luminosity is measured using the small angle Bremsstrahlung process ($ep \rightarrow ep\gamma$) in which the final state photon is detected in a calorimeter close to the beam-pipe at 103 m from the interaction region.

4 Event Selection

Preselection of the Dijet Sample with a High $\mathrm{p_t}$ Muon

The analysis is based on the event sample selected for the recent determination of the beauty cross section [5]. The data were recorded in 1999 and 2000 and correspond to an integrated luminosity of $48\,\mathrm{pb}^{-1}$. In [5] a detailed account of the event selection is given, e.g. of the triggering of events, of the selection of photoproduction and of many other aspects. The accepted range of negative four-momentum transfer squared Q^2 is restricted to $Q^2 < 1$ GeV^2 and the inelasticity y to 0.2 $< y <$ 0.8. Jets are reconstructed using the inclusive k_t algorithm [8, 9] in the p_t recombination scheme (see [10]), giving massless jets. The algorithm, with a distance parameter in the η-ϕ plane of $R = 1$, is applied to all hadronic final state particles using a combination of tracks and calorimeter energy deposits. The selection requires at least two jets with transverse energy $p_t^{jet_{1(2)}} > 7(6)$ GeV, of which at least one contains a muon candidate. Muons are selected in the angular range $35^\circ < \theta(\mu) < 130^\circ$, and are required to have transverse momenta $p_t^\mu > 2.5$ GeV. Only muon tracks are selected for which associated hits are found in both layers of the H1 vertex detector [6], thus providing high spatial track resolution close to the ep collision vertex. The selection cuts for the Dijet + Muon sample are summarized in table 1.

For the measurement of the beauty cross section [5], two observables were used to separate beauty events from charm events and light quark background, exploiting the large mass and the long lifetime of the b-quark, respectively. These quantities are used here to define a charm enriched sample and to check the fraction of charm events in the final selection.

1. The relative transverse momentum p_t^{rel} of the muon with respect to the axis of the associated jet.

2. The impact parameter δ of the muon, which is the distance of the track in the transverse plane with respect to the ep collision vertex.

The distributions of p_t^{rel} and δ for the selected dijet plus muon event sample are shown in fig. 5. The fractions of charm, beauty and uds events in the data are determined from a combined fit to the two-dimensional distribution of δ and p_t^{rel}. The fit uses the shapes of the distributions of beauty, charm and light quark events from the PYTHIA Monte Carlo simulation. The relative weights of all three components are adjusted such that the likelihood is maximized. The overall normalization of the summed contributions is adjusted to match the data. The result of this fit is also illustrated in fig. 5. Both the p_t^{rel} and δ data distributions are nicely described by the sum of the three contributions, which are also shown separately.

Selection of a Charm Enriched Sample

In order to enrich events containing charm quark decays a cut on the transverse momentum p_t^{rel} of the muon track relative to the momentum of the associated jet, $p_t^{rel} < 1\,\mathrm{GeV}$, is imposed. The final sample then contains 800 events. The combined fit of p_t^{rel} and δ leads to a charm fraction of $73 \pm 3\%$ in this region compared to $71 \pm 2\%$ (MC statistics) expected from the PYTHIA Monte Carlo simulation. The remaining background due to b and light quark ('uds') production is subtracted statistically, using the fractions as predicted in the PYTHIA Monte Carlo simulation. Note that this procedure of selecting a charm enriched sample is independent of the production mechanism but only depends on the decay and fragmentation properties of the charm hadrons. The number of studied jets is equal to the number of events in the charm enriched sample.

Selection of a Dijet Sample

For comparison a dijet event sample is selected which fulfills the same jet selection criteria as the charm sample except for the requirement of a high p_t muon. Photoproduction is ensured by the presence of the scattered beam lepton in the low angle tagging device which selects $Q^2 < 0.01\,\mathrm{GeV}^2$ and also serves for triggering. The inelasticity y is restricted to the range $0.3 < y < 0.65$. The event selection cuts are summarized in table 1. This event sample is dominated by the production of light quarks ($\sim 75\%$). The two jets with the highest p_t are studied in each event.

5 Monte Carlo Simulations

Monte Carlo event samples for the processes $ep \rightarrow ec\bar{c}X$, $ep \rightarrow eb\bar{b}X$ and light quark production are generated using the PYTHIA program [3] which is based on leading order QCD and parton showers. PYTHIA simulates direct and resolved photon processes and also includes excitation processes, in which one heavy quark (c or b) originates from the resolved photon or the proton. PYTHIA is run in an inclusive mode and generates all the above processes using massless matrix elements. The Peterson fragmentation function [15] is used for the hadronisation of the heavy quarks. The CTEQ5L [11] parton densities are used for the proton and those of GRVG-LO [12] for the photon. The light quark sample is used to simulate the background from fake muons, i.e. hadrons misidentified as muons, and decays of light mesons into muons.

The program CASCADE [13], a Monte Carlo generator which implements the CCFM parton evolution equation [14], uses unintegrated parton densities JS2001 and of-shell matrix elements is used for a cross check. For comparison with the dijet sample an inclusive PYTHIA data set is used. The generated events after fragmentation are passed through a detailed simulation of the H1 detector and the same reconstruction software is used as for the data.

6 Results

In figures 6 and 7 distributions are shown for the charm enriched and the dijet samples. where the data are compared to the PYTHIA Monte Carlo simulations. The overall normalization of PYTHIA in the charm enriched sample is adjusted to match the data, while the relative fractions of charm, beauty and light quark events as predicted by PYTHIA. The fraction x_γ^{obs} of the photon energy entering the hard interaction is estimated using the observable

$$x_\gamma^{obs} = \frac{\sum_{Jet_1}(E - p_z) + \sum_{Jet_2}(E - p_z)}{\sum_h (E - p_z)},$$

where the sums in the numerator run over the particles associated with the two jets and that in the denominator over all detected hadronic final state particles. For the direct process (figure 1a), x_γ^{obs} approaches unity, since the hadronic final state consists of only the two hard jets and the proton remnant in the forward region, which however contributes little to $\sum_h (E - p_z)$. In resolved processes x_γ^{obs} can be small.

The distributions of the averaged integrated jet shapes $\langle\psi(r)\rangle$ as functions of the cone radius r are shown in figures 9 and 10 for the light quark dominated dijet sample and for the charm sample, respectively. The distributions are presented for two separate regions of the variable x_γ^{obs}. For the dijet sample both selected jets enter the distributions. In the charm sample the jet tagged by the muon is initiated by a charm quark in 95% of the events according to the PYTHIA Monte Carlo simulation. The other jet is studied and enters the jet shape distributions. The background in this sample from beauty and light quark events is subtracted from the $\psi(r)$ distribution before calculating the average $\langle\psi(r)\rangle$ (see figure 8). In figures 9 and 10 the PYTHIA predictions are shown with the data. In addition to the total prediction the curves for the direct and resolved photon events are shown separately. For the dijet sample good agreement between data and PYTHIA prediction can be observed both at low and high x_γ^{obs}. For charm the data are described well by the PYTHIA prediction at high x_γ^{obs} but disagreement is observed in the region of $x_\gamma^{obs} \leq 0.75$. In this region the data show approximately the same shape as in the region $x_\gamma^{obs} > 0.75$. The PYTHIA simulation however predicts a slower rise of $\langle\psi(r)\rangle$ due to the presence of gluon jets in the resolved photon sample. The charm data are shown again in figure 11 with the prediction of the CASCADE model, where no explicit resolved component is generated. The CASCADE prediction describes the data perfectly in the high x_γ^{obs} region and is closer to the data in the low x_γ^{obs} region than PYTHIA. In figures 12 and 13 the averaged integrated jet shapes at $r/R = 0.5$ are shown for the dijet and the charm samples as a functions of the pseudorapidity of the jet, its transverse momentum, energy and x_γ^{obs}. PYTHIA describes the dijet data well everywhere. For the charm data the distribution as a function of pseudorapidity and p_t^{jet} is well described, however deviations are seen at high jet energy and low x_γ^{obs}.

In figure 14 the charm data are shown again with the predictions from the PYTHIA and CASCADE models. CASCADE is somewhat closer to the data at low x_γ^{obs}, but at high jet energy CASCADE predicts the same value as PYTHIA.

In figure 14 a result from PYTHIA omitting the simulation of interactions between the photon and proton remnants ('multiple interactions') is also shown. This has a small effects on the jet shapes: the simulation without multiple interactions is closer to the data at low x_γ^{obs}, while the description at high x_γ^{obs} remains good. Various systematic checks have been carried out for the charm sample. Variation of the Peterson fragmentation parameter ϵ between 0.03 and 0.08 (default value 0.058) did not change the distributions. Variation of the background due to b quarks and light quarks by $\pm 20\%$, variation of the energy scale of the clusters by $\pm 5\%$ and jet axis smearing by 2° led to a systematical error of about 0.35% which is smaller than the statistical error.

A direct comparison of the jet shapes in charm and dijet data is shown in figures 15 and 16. A clear difference between the data is seen at low values of x_γ^{obs} between the shapes of charm and dijet events as function of r/R. In figure 16 the dependence of $\langle\psi(r)\rangle$ at $r/R = 0.5$ is compared. The difference between dijet and charm events is seen at large values of the pseudorapidity, i.e. in the forward direction, for large jet energies and at low x_γ^{obs}.

7 Conclusions

Jet shapes are studied in a charm dijet photoproduction sample with the H1 detector at HERA. With the final selection cuts, about 71% of the sample is due to charm events (according to the simulation), the rest is due to beauty and light quark background with about equal shares. The background is subtracted statistically to obtain a pure charm sample. The charm events are tagged by a high p_t muon which is associated to one of the jets and thus identifies this jet as being charm quark initiated. The jet not containing the muon is studied and compared to predictions by a PYTHIA Monte Carlo simulation which contains direct and resolved photon events. The resolved component in PYTHIA is dominated by charm excitation, where in addition to the charm quark jet (tagged by the muon) a gluon initiated jet is expected, which has a different shape than the charm jet. In the charm data sample the jet shapes are however found to be similar in direct and resolved photon enriched samples, while PYTHIA predicts significant differences due to the different mixture of charm quark and gluon jets in direct and resolved photon events. For comparison a dijet sample was selected without the high p_t muon, which is dominated by light quark production. Here the jet shapes are significantly different in direct and resolved photon enriched data samples and in agreement with PYTHIA, which predicts a large fraction of gluon jets in the resolved photon sample. We conclude that the discrepancy between the charm data and PYTHIA observed for the jet shapes in the resolved photon region indicates a lack of understanding of the charm production process in the resolved photon region.

Acknowledgements

We are grateful to the HERA machine group whose outstanding efforts have made this experiment possible. We thank the engineers and technicians for their work in constructing and maintaining the H1 detector, our funding agencies for financial support, the DESY technical staff for continual assistance and the DESY directorate for support and for the hospitality which they extend to the non DESY members of the collaboration.

References

[1] G. Alexander *et al.* [OPAL Collaboration], Z. Phys. C **69** (1996) 543.

[2] R.K. Ellis, W.J. Stirling and B.R. Webber, QCD and Collider Physics, Cambridge University Press (1996)

[3] T. Sjostrand, Comput. Phys. Commun. **82** (1994) 74.

[4] I. Abt *et al.* [H1 Collaboration], Nucl. Instrum. Meth. A **386** (1997) 310 and 348.

[5] A. Aktas *et al.* [H1 Collaboration], arXiv:hep-ex/0502010.

[6] D. Pitzl *et al.*, Nucl. Instrum. Meth. A **454**, 334 (2000) [arXiv:hep-ex/0002044].

[7] S. Catani, Yu. Dokshitzer, M.H.Seymour and B.R. Webber, Nucl. Phys. B 406 (1993) 187.

[8] S.D. Ellis and D.E. Soper, Phys. Rev. D **48** (1993) 3160 [hep-ph/9305266].

[9] S. Catani, Y.L. Dokshitzer, M.H. Seymour and B.R. Webber, Nucl. Phys. B **406** (1993) 187.

[10] J.M. Butterworth, J.P. Couchman, B.E. Cox and B.M. Waugh, Comput. Phys. Commun. **153** (2003) 85 [hep-ph/0210022].

[11] L. Lai *et al.* [hep-ph/9903282].

[12] M. Glück, E. Reya and A. Vogt, Phys. Rev.D45, 3986(1992); Phys. Rev. D46, 1973 (1992).

[13] H. Jung and G. P. Salam, Eur. Phys. J. C **19** (2001) 351 [hep-ph/0012143];
H. Jung, Comput. Phys. Commun. **143** (2002) 100 [hep-ph/0109102].

[14] M. Ciafaloni, Nucl. Phys. B **296** (1988) 49;
S. Catani, F. Fiorani and G. Marchesini,
Phys. Lett. B **234** (1990) 339, Nucl. Phys. B **336** (1990) 18;
G. Marchesini, Nucl. Phys. B **445** (1995) 49.

[15] C. Peterson, D. Schlatter, I. Schmitt, and P.M. Zerwas, Phys. Rev. D 27 (1983) 105.

[16] A.D. Martin, R.G. Roberts and W.J. Stirling, Phys.Lett. B354, 155 (1995); A.D. Martin, R.G. Roberts, W.J. Stirling and R.S. Thorne, Eur. Phys. J. C4 (1998) 463.

	Dijet+Muon	Dijet
Q^2 [GeV^2]	< 1	< 0.01
y	0.2 ... 0.8	0.3 ... 0.65
# jets	≥ 2	
p_t^{jet} [GeV]	$> 7(6)$	
$\lvert\eta_{lab}^{jet}\rvert$	< 1.7	< 1.7
p_t^{μ} [GeV]	> 2.5	–
Trigger	Muon and jets	E-Tagger

Table 1: Selection cuts for the photoproduction dijet+muon and dijet data samples.

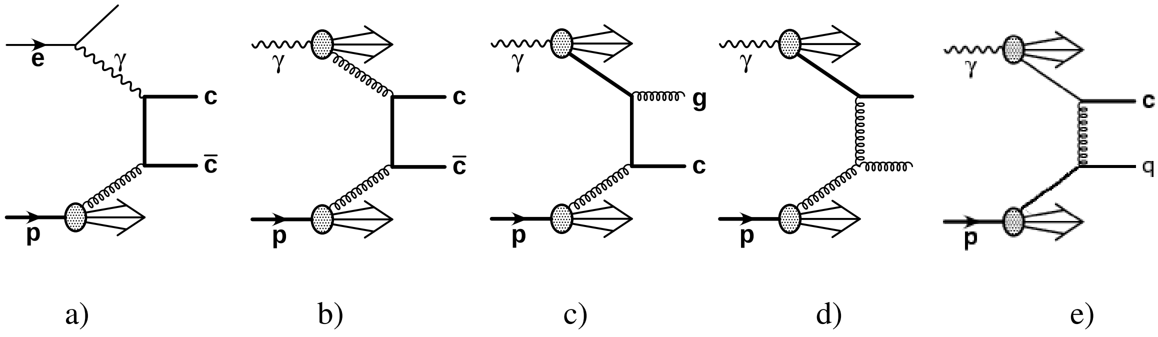

Figure 1: Charm quark production processes in leading order pQCD.

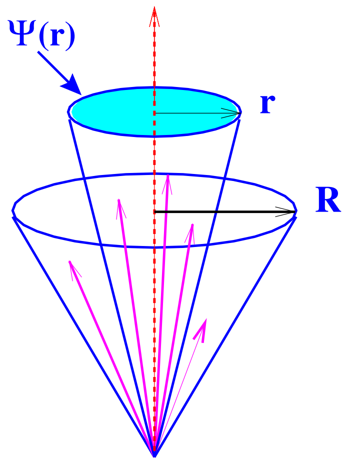

Figure 2: Definition of jet cones.

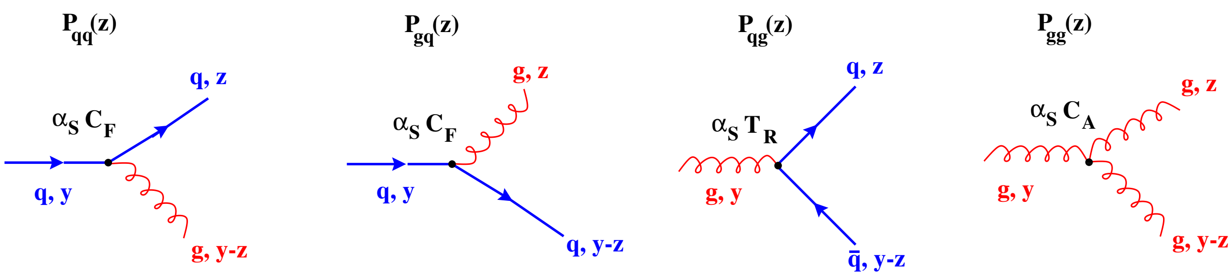

Figure 3: Branching processes of quarks and gluons.

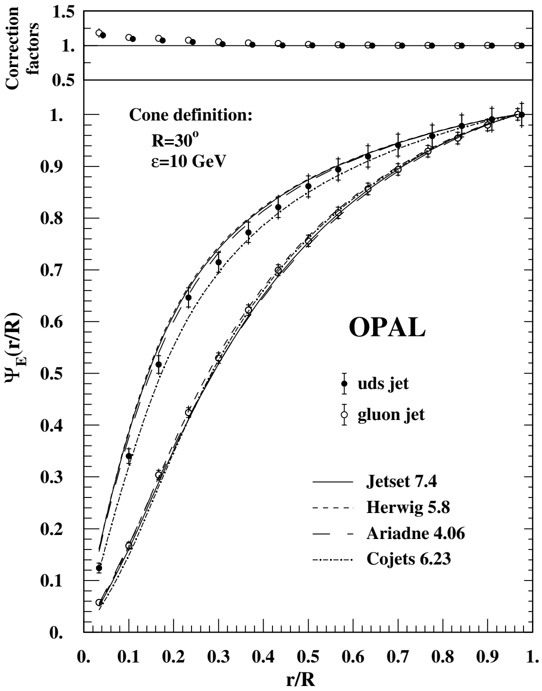

Figure 4: $\langle\psi(r)\rangle$ Spectra for light quark and gluons jets as measured by OPAL [1].

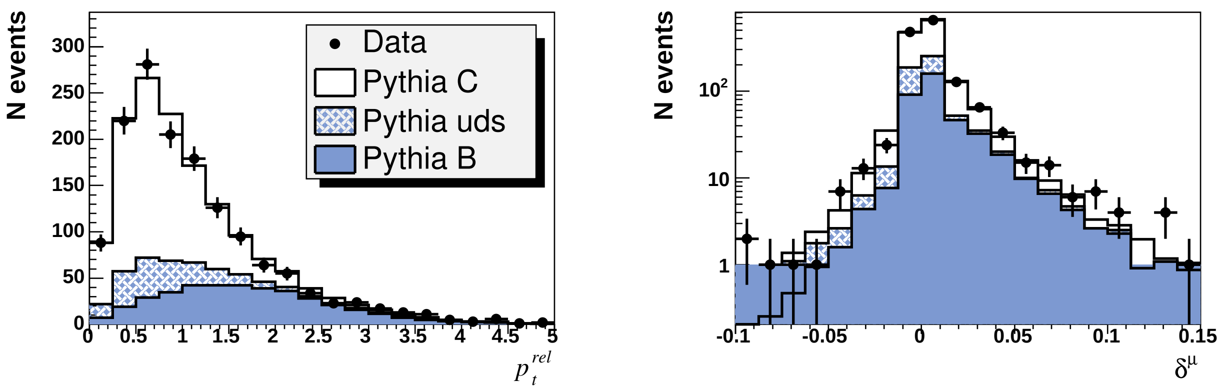

Figure 5: Determination of the charm fraction. The distributions of the relative momentum p_t^{rel} of the muon w.r.t the jet-axis and the impact parameter δ of the muon track w.r.t the event vertex are shown. The solid line shows the expectation from the Monte Carlo simulation. The light (dark) shaded histograms indicate the contributions from light quark (beauty) events obtained from a fit to the data.

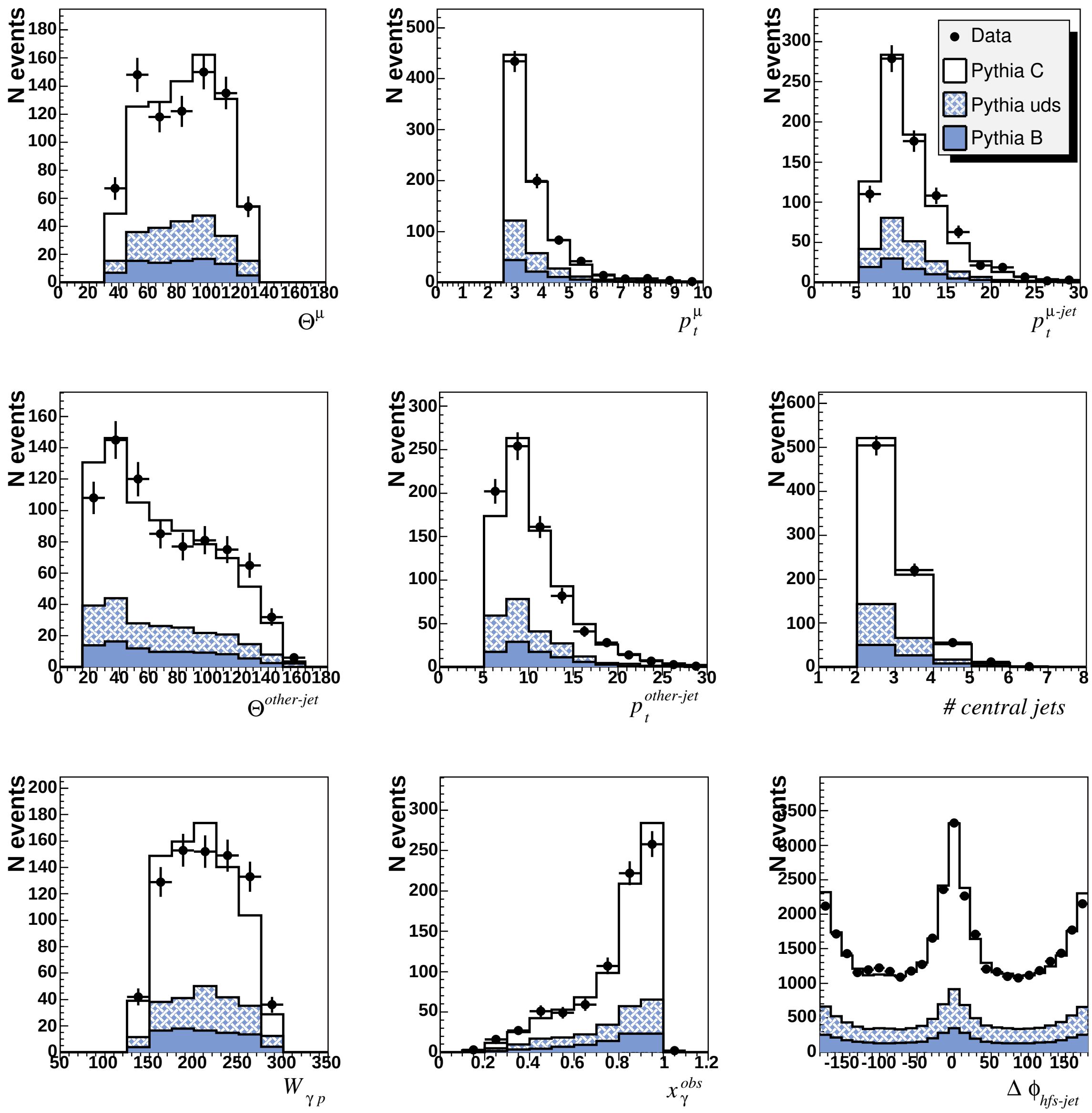

Figure 6: Control distributions for the charm enriched dijet plus muon sample. The data (points) are compared with the PYTHIA Monte Carlo simulation (lines). The remaining background from b quark and light quarks with fake muons ('uds') is shown separately. for the muon polar angle θ_μ and transverse momentum p_t^μ, the transverse momentum $p_t^{\mu-jet}$ of the jet associated to the muon, the polar angle $\theta^{other\ jet}$ and transverse momentum $p_t^{other\ jet}$ of the jet not associated to the muon, the number of jets with $p_t^{jet} > 2.5\,\mathrm{GeV}$, the photon proton centre-of-mass-energy $W_{\gamma p}$, the quantity x_γ^{obs} and the hadronic energy flow, i.e. the hadronic particles as a function of the azimuthal angle difference $\Delta\Phi$ with respect to the axis of the 'other' jet.

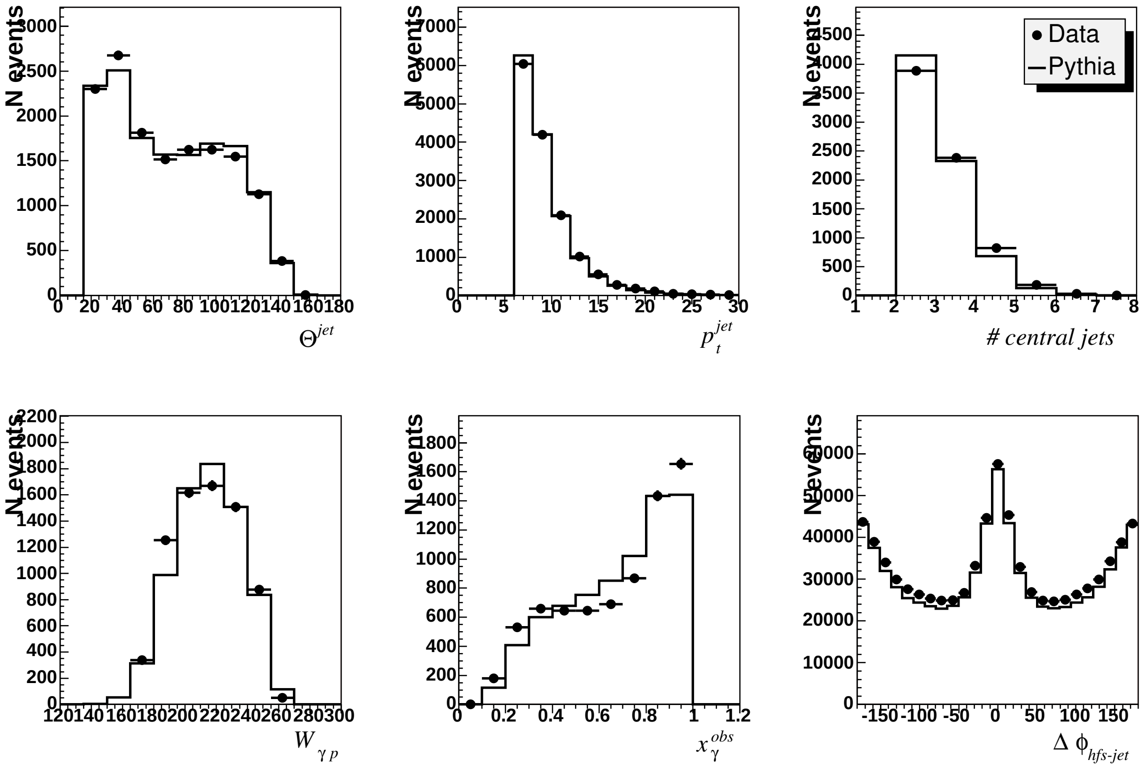

Figure 7: Control distributions for the dijet sample. The data (points) are compared with the PYTHIA Monte Carlo simulation (lines) for the polar angle θ^{jet} and transverse momentum p_t^{jet} of the selected jets, the number of jets with $p_t^{jet} > 2.5\,\mathrm{GeV}$, the photon proton centre-of-mass-energy $W_{\gamma p}$, the quantity x_γ^{obs} and the hadronic energy flow, i.e. the hadronic particles as a function of the azimuthal angle difference $\Delta\Phi$ with respect to the jet axis.

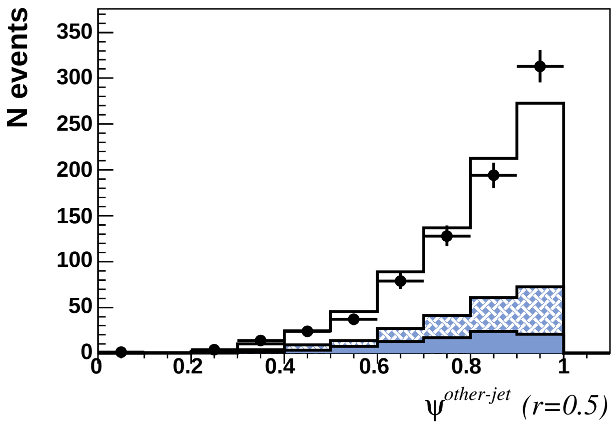

Figure 8: Distribution of $\psi(r)$ for a cone radius of $r/R = 0.5$ before background subtraction compared with the PYTHIA simualtion. The shaded area represents the background due to b initated jets and the dotted area due to light quark jets.

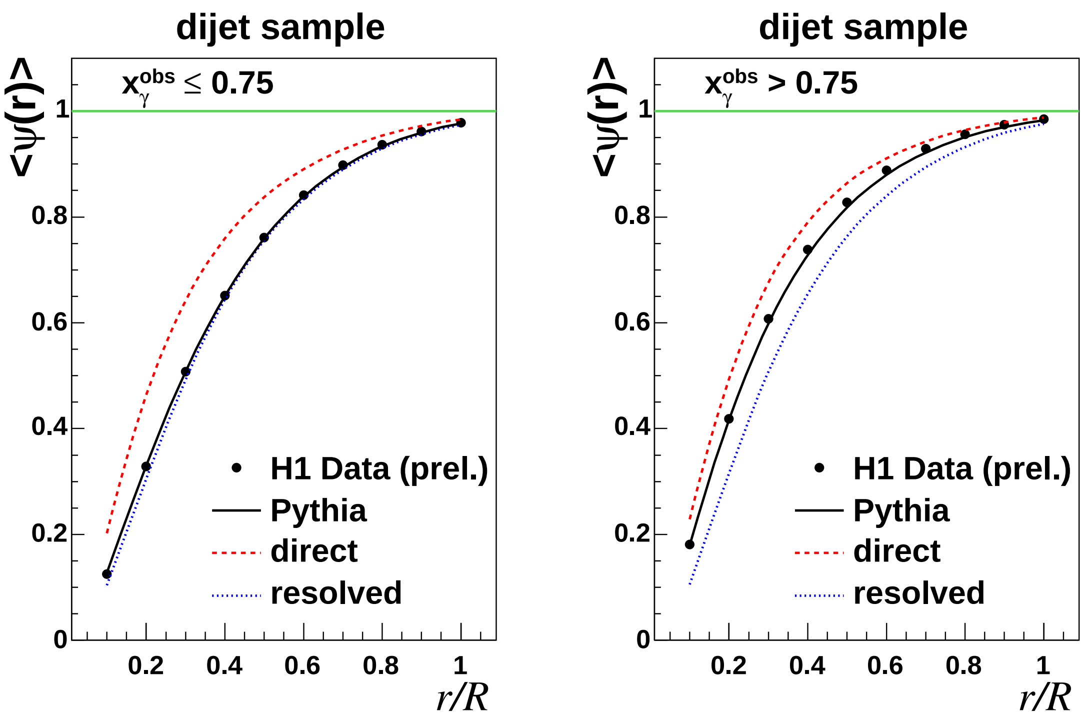

Figure 9: $\langle\psi(r)\rangle$ for the dijet event sample for two different regions of x_γ^{obs}. The data are compared to the prediction from PYTHIA. The expected curves for direct photon (dashed) and resolved photon (dotted) events from PYTHIA are shown separately.

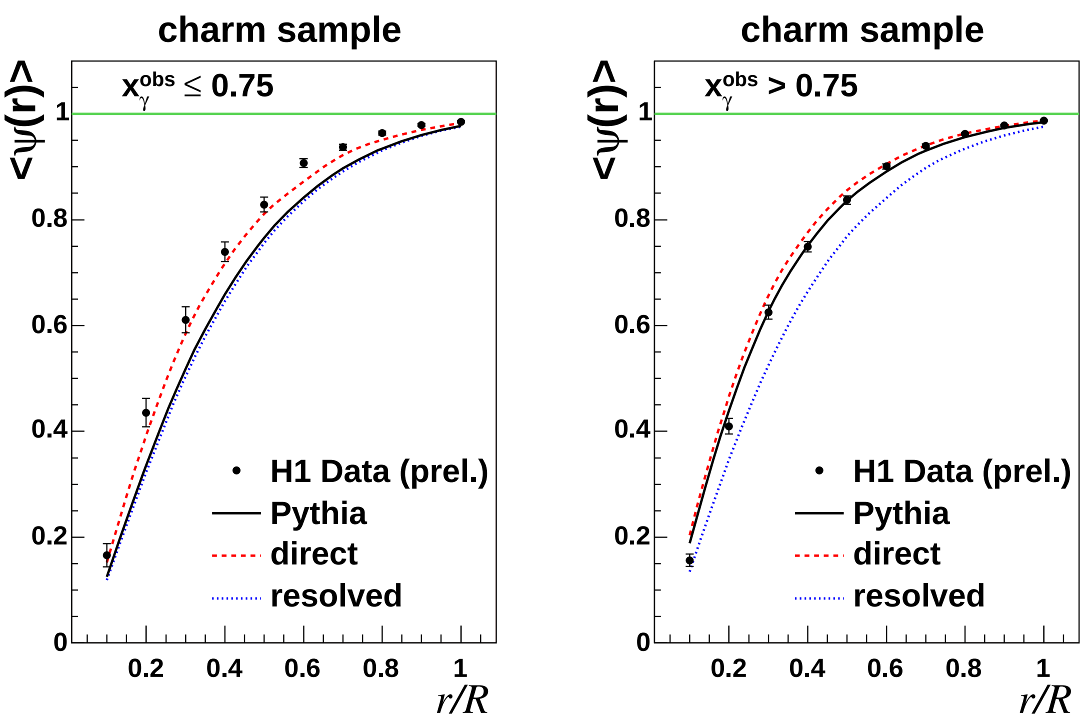

Figure 10: $\langle\psi(r)\rangle$ for the charm event sample for two different regions of x_γ^{obs}. The data are compared to the prediction from PYTHIA. The expected curves for direct photon (dashed) and resolved photon (dotted) events from PYTHIA are shown separately.

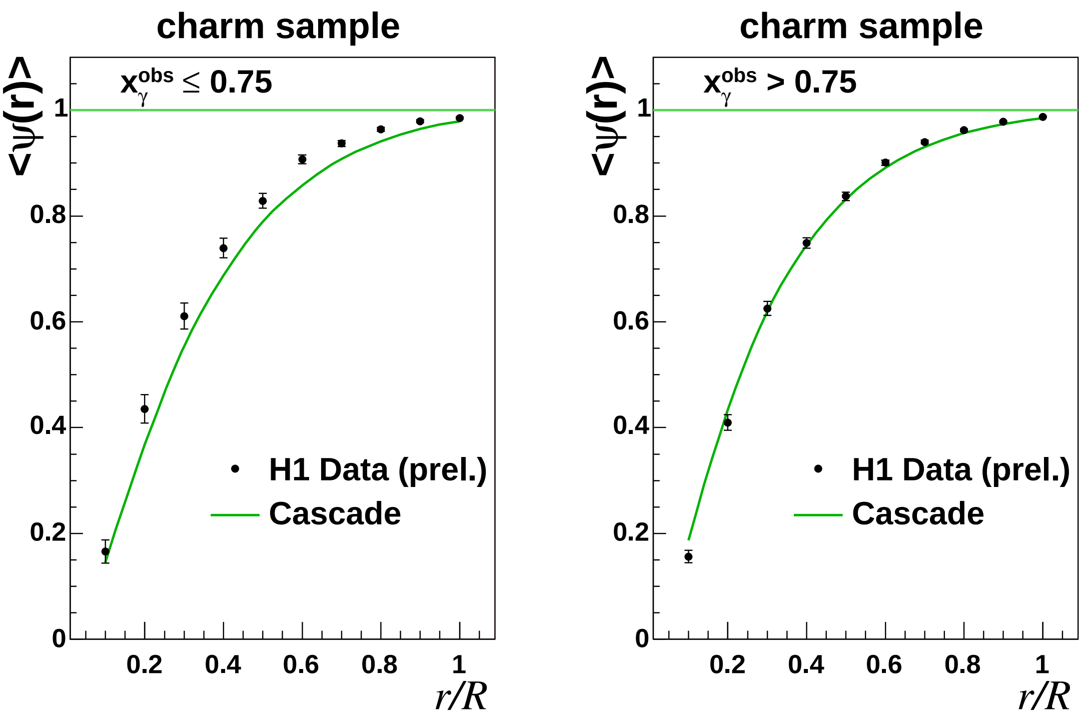

Figure 11: $\langle\psi(r)\rangle$ for the charm event sample for two different regions of x_γ^{obs}. The data are compared to the CASCADE prediction.

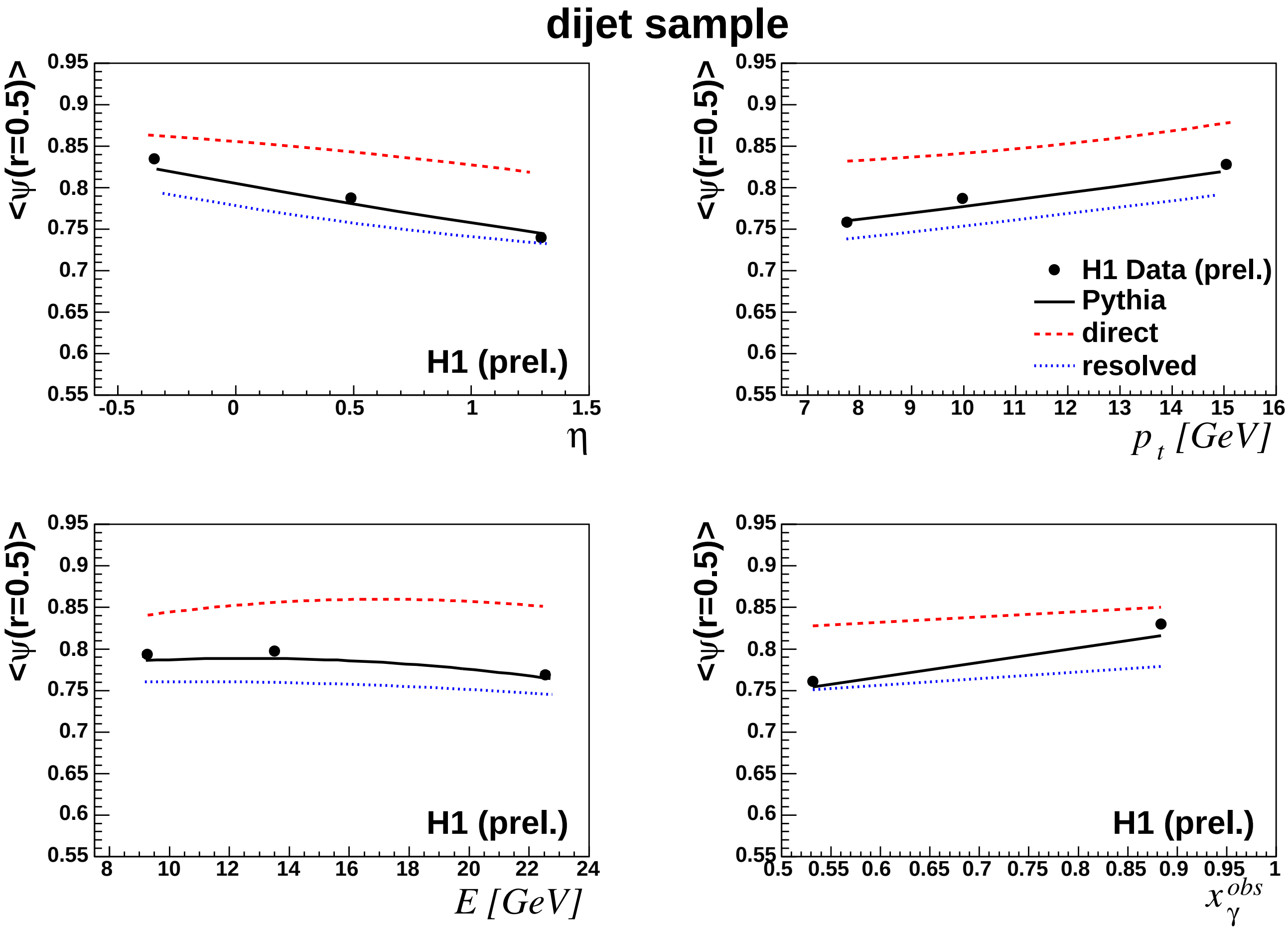

Figure 12: Differential distributions of $\langle\psi(r/R = 0.5)\rangle$ as functions η_{jet}, p_t^{jet}, E_{jet} and x_γ^{obs} for the dijet event sample. The predictions from the PYTHIA simulation are compared with the data. The expected curves for direct photon (dashed) and resolved photon (dotted) events from PYTHIA are shown separately.

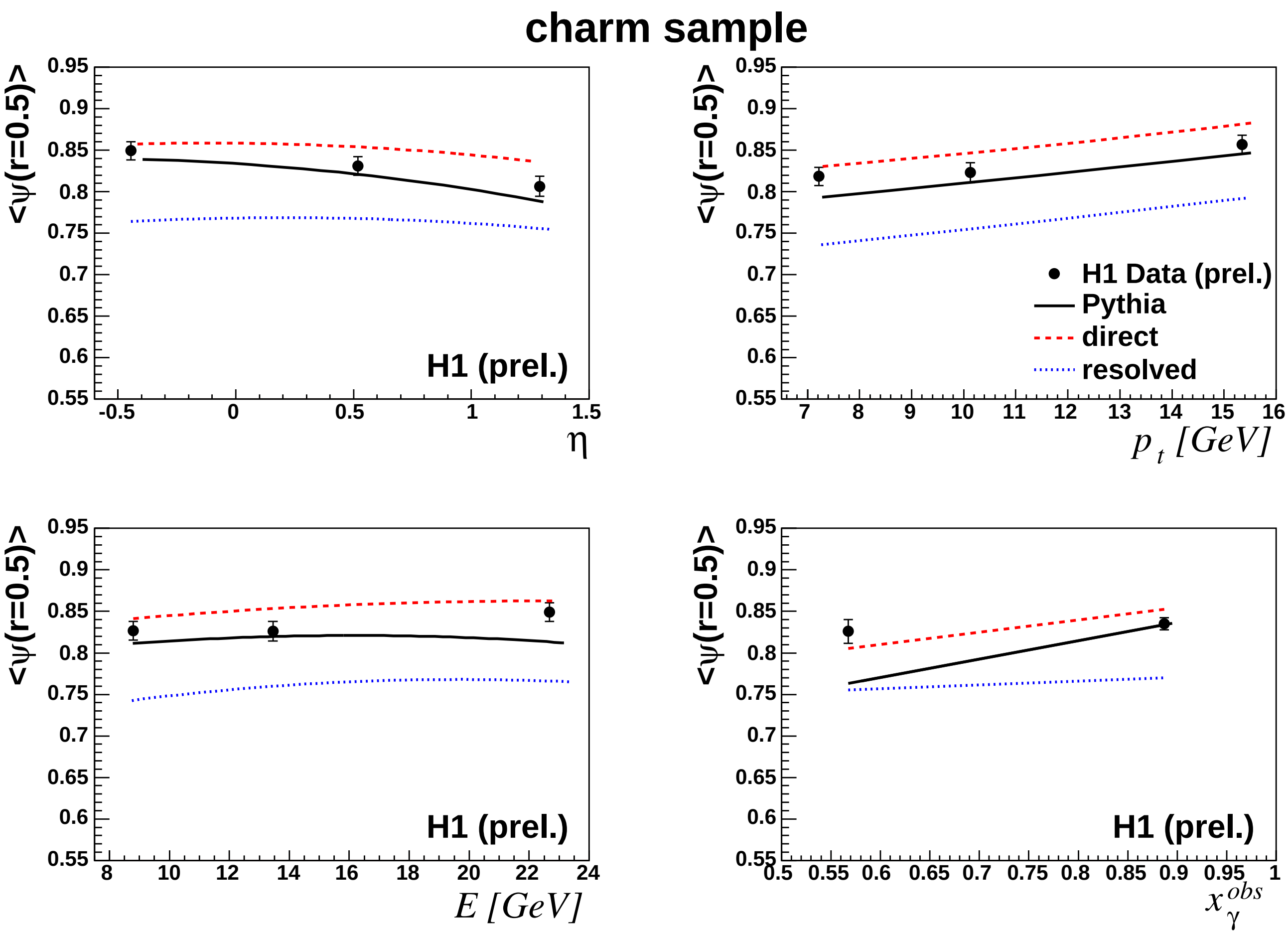

Figure 13: Differential distributions of $\langle\psi(r/R = 0.5)\rangle$ as functions of η_{jet}, p_t^{jet}, E_{jet} and x_γ^{obs} for the charm event sample. The predictions from PYTHIA are compared with the data. The expectations for direct photon (dashed) and resolved photon (dotted) events from PYTHIA are shown separately. Also shown is the expectation for charm quarks from the CASCADE simulation (dash-dotted line).

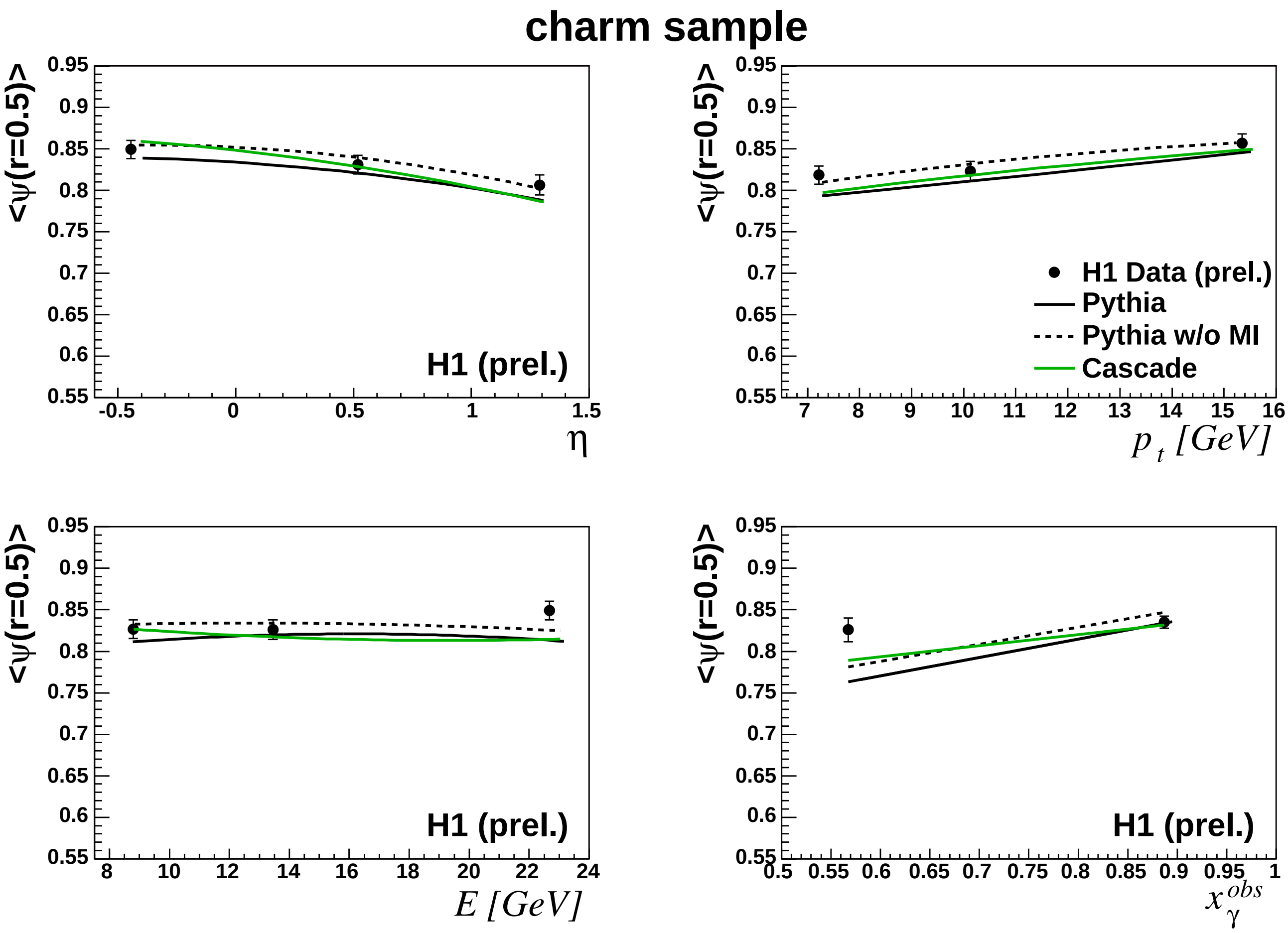

Figure 14: Differential distributions of $\langle\psi(r/R = 0.5)\rangle$ as functions of η_{jet}, p_t^{jet}, E_{jet} and x_γ^{obs} for the charm event sample. The predictions from PYTHIA with and without multiple interactions and CASCADE are compared with the data.

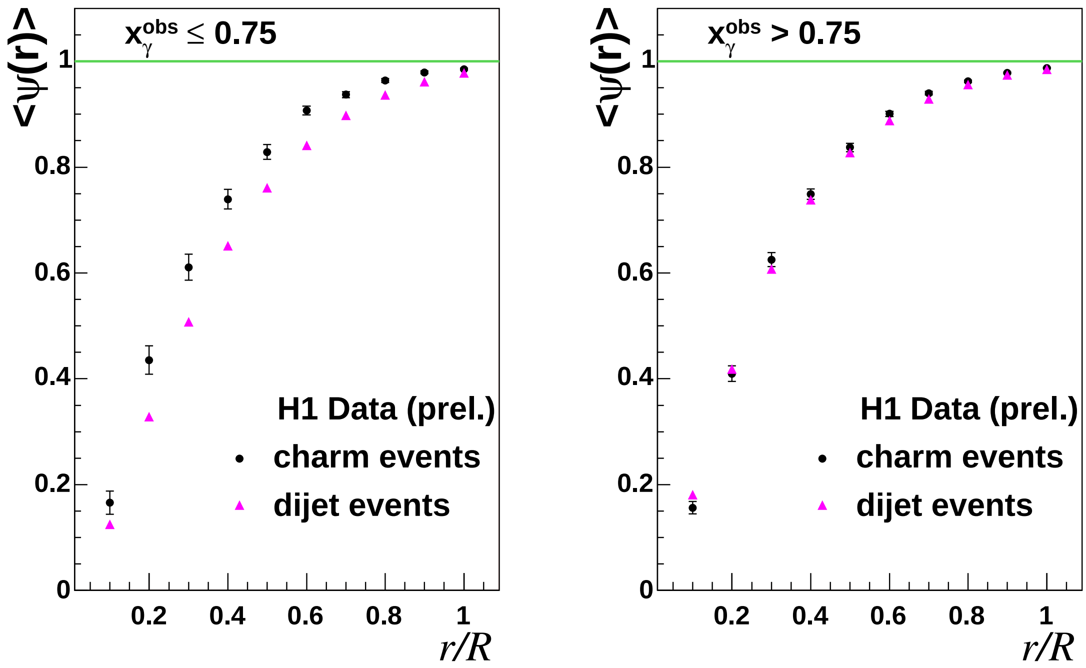

Figure 15: $\langle\psi(r)\rangle$ for the charm and dijet data samples in two different regions of x_γ^{obs}.

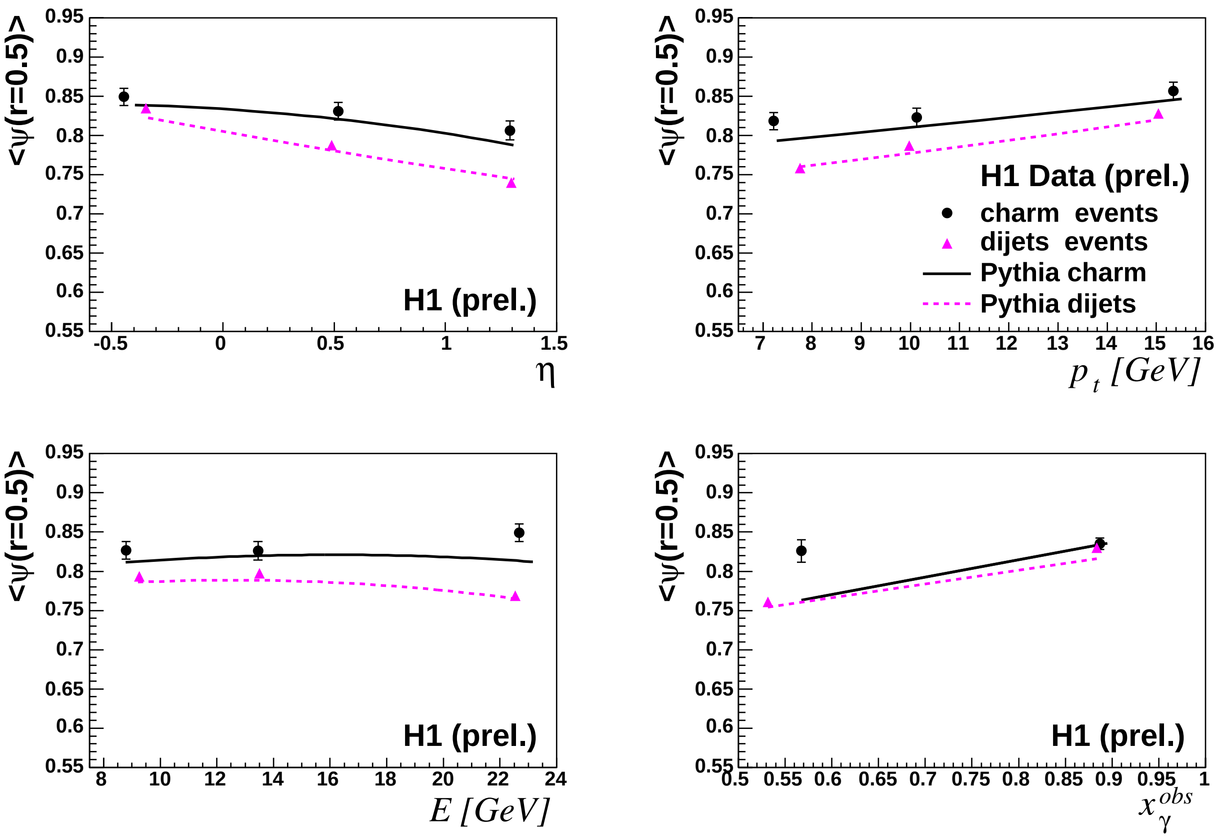

Figure 16: Differential distributions of $\langle\psi(r/R = 0.5)\rangle$ as functions of η_{jet}, p_t^{jet}, E_{jet} and x_γ^{obs} for the charm and dijet event samples. The predictions from PYTHIA for charm and dijets are shown with the data.